Solving Poisson equation with Successive Overrelaxation method (SOR)

Gabriela Pyda

28 November 2025

1 Introduction

The primary objective of this laboratory is to solve the Poisson equation for the electric potential $V(\vec{r})$ in a two-dimensional space. The Poisson equation is a partial differential equation of elliptic type that relates the potential to the charge density distribution $\rho(x, y)$. In 2D Cartesian coordinates defined on a square domain $(x, y) \in [-L, L]\times[-L, L]$, the equation takes the form of Formula (1), where ε represents the dielectric permittivity of the medium. In this study, the charge density is modeled by the function $\rho(x, y) = A_\rho xye^{-(x^2+y^2)}$, where A_ρ is an amplitude coefficient.

$$\nabla^2 V = \frac{\partial^2 V}{\partial x^2} + \frac{\partial^2 V}{\partial y^2} = -\frac{\rho(x, y)}{\varepsilon} \tag{1}$$

To obtain a unique solution, Formula (1) must be supplemented with appropriate boundary conditions (BCs) on the edges of the computational domain. Two types of boundary conditions are considered:

1. **Dirichlet Boundary Conditions**, where the value of the potential V is explicitly specified on the boundary. In the general case, non-homogeneous conditions are applied where V varies along the edges (the sinusoidal profiles were used in the experiment).

2. **Neumann Boundary Conditions**, where the normal derivative of the potential is specified. For instance, on the right boundary ($x = x_{max}$), a condition of the form $\frac{\partial V}{\partial x} = 0$ may be imposed, physically corresponding to a zero electric field component normal to the surface.

Since analytical solutions for arbitrary charge distributions and boundary conditions are often hard to calculate, numerical methods such as the Finite Difference Method (FDM) are employed to approximate the solution on a discrete grid.

2 Numerical Methods and Algorithms

2.1 Discretization and the Finite Difference Method

The continuous domain is discretized into a square mesh of $N \times N$ nodes. The spatial step size is uniform in both directions, given by $\Delta = \frac{2L}{N-1}$. The continuous potential

$V(x, y)$ and charge density $\rho(x, y)$ are approximated by their discrete values $V_{i,j}$ and $\rho_{i,j}$ at grid points (x_i, y_j).

Using the Taylor series expansion, the second-order partial derivatives in the Laplace operator are approximated using the three-point central difference formula (Formula (2)). Substituting these into the Poisson equation yields the discrete system of linear equations presented in the Formula (3).

$$\frac{\partial^2 V}{\partial x^2} \approx \frac{V_{i+1,j} - 2V_{i,j} + V_{i-1,j}}{\Delta^2}, \quad \frac{\partial^2 V}{\partial y^2} \approx \frac{V_{i,j+1} - 2V_{i,j} + V_{i,j-1}}{\Delta^2} \tag{2}$$

$$V_{i+1,j} + V_{i-1,j} + V_{i,j+1} + V_{i,j-1} - 4V_{i,j} = -\frac{\rho_{i,j}\Delta^2}{\varepsilon} \tag{3}$$

2.2 The Successive Over-Relaxation (SOR) Algorithm

To solve the large sparse system of equations resulting from discretization, iterative relaxation methods are used. The basic update rule isolates $V_{i,j}$ on the left-hand side in Formula (4).

$$V^*_{i,j} = \frac{1}{4}\left(V_{i+1,j} + V_{i-1,j} + V_{i,j+1} + V_{i,j-1} + \frac{\rho_{i,j}\Delta^2}{\varepsilon}\right) \tag{4}$$

The Successive Over-Relaxation (SOR) method improves the convergence rate of this basic scheme (which corresponds to the Gauss-Seidel method when used directly) by introducing a relaxation parameter $\omega \in (0, 2)$. The update rule for the potential at iteration $k+1$ is presented in Formula (5). Substituting $V^*_{i,j}$, the explicit formula used in the algorithm is showed in Formula (6).

$$V^{(k+1)}_{i,j} = (1-\omega)V^{(k)}_{i,j} + \omega V^*_{i,j} \tag{5}$$

$$V^{(k+1)}_{i,j} = (1-\omega)V^{(k)}_{i,j} + \frac{\omega}{4}\left(V_{i+1,j} + V_{i-1,j} + V_{i,j+1} + V_{i,j-1} + \frac{\rho_{i,j}\Delta^2}{\varepsilon}\right) \tag{6}$$

When $\omega = 1$, the method reduces to the Gauss-Seidel algorithm. Values of $1 < \omega < 2$ typically accelerate convergence (over-relaxation).

2.3 Implementation of Boundary Conditions

- **Dirichlet BCs**, where the values of $V_{i,j}$ at the boundary nodes (indices $i = 0, i = N-1, j = 0, j = N-1$) are fixed during initialization and are not updated during the relaxation loop. The choice is based on the sinusoidal shape of the boundary values.

- **Neumann BCs**, where, for a condition $\frac{\partial V}{\partial x} = 0$ at the right boundary ($i = N-1$), a finite difference approximation is used. Using a two-point backward difference scheme from a Formula (7). This condition is enforced after every iteration of the relaxation loop by copying the values from the column $N-2$ to the boundary column $N-1$.

$$\frac{V_{N-1,j} - V_{N-2,j}}{\Delta} = 0 \implies V_{N-1,j} = V_{N-2,j} \tag{7}$$

2.4 Stopping Criterion

To determine whether the iterative process has converged, a physical criterion based on the electric field energy functional S is employed with use of the Formula (8), where $\vec{E} = -\nabla V$.

$$S = \int d^2r \left(\frac{1}{2} |\vec{E}|^2 - V \frac{\rho}{\varepsilon} \right) \tag{8}$$

In the discrete formulation, the integral is approximated by a summation over the grid. The derivatives for $\vec{E}$ are calculated using central differences. The iterations are stopped when the relative change in S between consecutive steps falls below a specified tolerance TOL, which is stated in the Formula (9).

$$\delta = \left| \frac{S_{k+1} - S_k}{S_k} \right| < TOL \tag{9}$$

2.5 Error Estimation

After convergence, the correctness of the solution is verified by calculating the local residual error at each node. This involves substituting the computed potential back into the discrete Poisson equation and measuring the difference between the left- and right-hand sides.

3 Results

Each part of the experiment operates on common initial parameters: $L = 4$, $N = 100$, $V_{max} = 1$, $\epsilon = 1$, $K_{max} = 10^4$ and $TOL = 10^{-8}$.

3.1 Initial test of correctness

Initial conditions for testing the correctness of the algorithm operated on additional parameters $A\rho = 0$, $k_1 = 1$, $k_2 = -1$, $k_3 = 1$, $k_4 = -1$ and $\omega = 1.5$. This parametrization allows to neglect the outer charge effects and depend only on the field generated through boundary conditions. The results are present in Figure 1.

It is visible that potential spread evenly and symmetrically, following its initial placement coming from boundary conditions. The error proves that the calculations were the most stable on diagonal of the mesh, while the parts which were the most distant from the boundaries and the diagonal have the highest error rate.

3.2 Variant with Neumann BC

The next step is to extend the initial test case with implementation of Neumann BC. The results are visible in Figure 2.

The Neumann BC significantly abrupted the initial state of the potential and visibly decreased the impact of the initial potential present in the highest values of x. Also the error proves that region mostly affected by the chosen BC has the biggest calculation error.

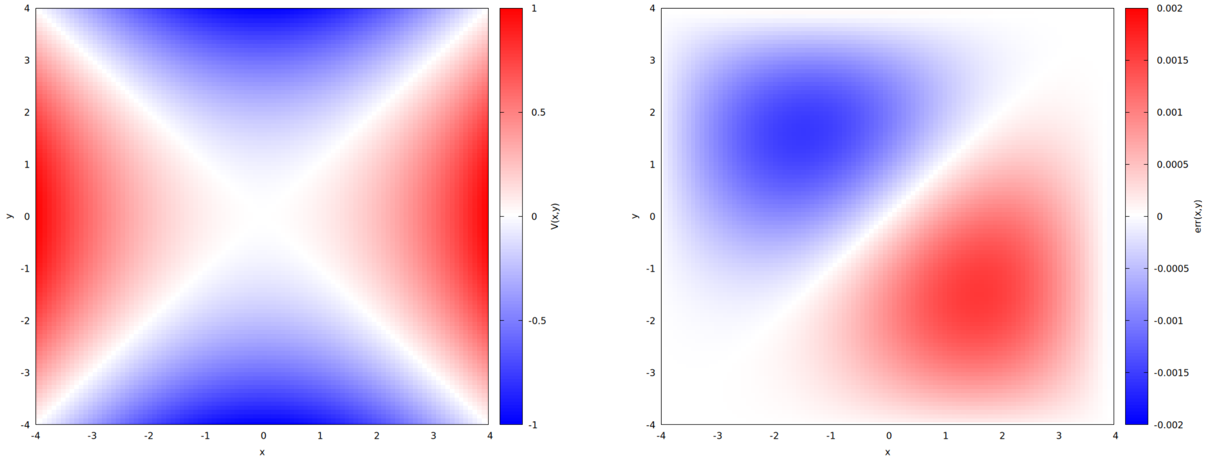

(a) Potential distribution

(b) Error $\nabla^2 V - \frac{\rho}{\epsilon}$

Figure 1: Visualization of potential and its error for $k_1 = 1$, $k_2 = -1$, $k_3 = 1$ and $k_4 = -1$

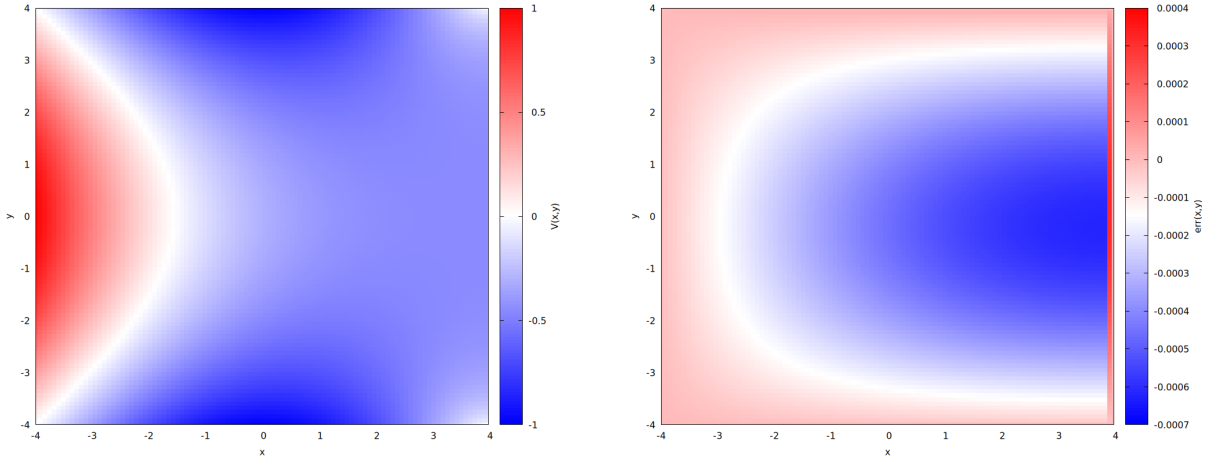

(a) Potential distribution

(b) Error $\nabla^2 V - \frac{\rho}{\epsilon}$

Figure 2: Visualization of potential and its error for Neumann BC

3.3 Impact of ω on the functional S

Another part of the laboratory was to analyze the performance of the SOR algorithm depending on convergence parameter ω. The results are shown in Figure 3.

For smaller values, the value of functional decreased significantly slower, requiring longer computation time and obtaining lower inter-iteration changes. This shows that the choice of *omega* may be important in obtaining the most optimal time of simulation.

3.4 Enabling charge density A_ρ

The last part of the experiment was to check the behavior of the potential field in existence of a charge and considering it in both homogeneous ($k_1 = k_2 = k_3 = k_4 = 0$) and inhomogeneous BC (as initial ones). The results for homogeneous field distribution are present in Figure 4, while the inhomogeneous conditions are present in Figure 5.

The homogeneous BC resulted in oddly distributed potential field, which seems to imply the bipolar nature of charge (which isn't true of course). The error also follows the

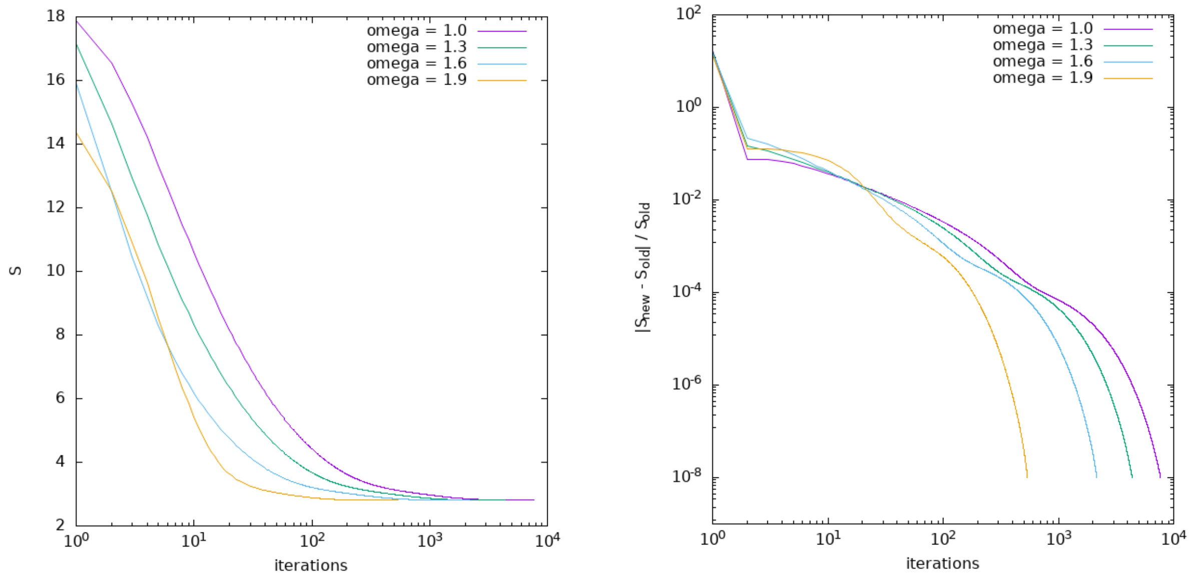

(a) SOR functional S

(b) Change $|\frac{S_{new}-S_{old}}{S_{old}}|$

Figure 3: Visualization of SOR functional's evolution over iterations

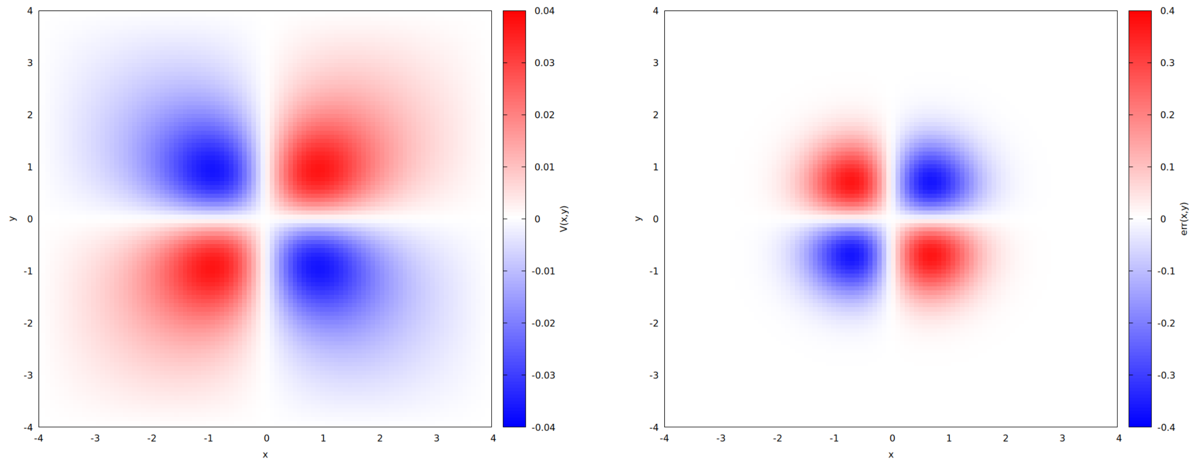

(a) Potential distribution

(b) Error $\nabla^2 V - \frac{\rho}{\epsilon}$

Figure 4: Visualization of potential and its error for homogeneous BC

patters. This experiment proves the significance of proper BC choice. For inhomogeneous BC, the potential closely resembles the initial result (Figure 1.(a))

4 Conclusions

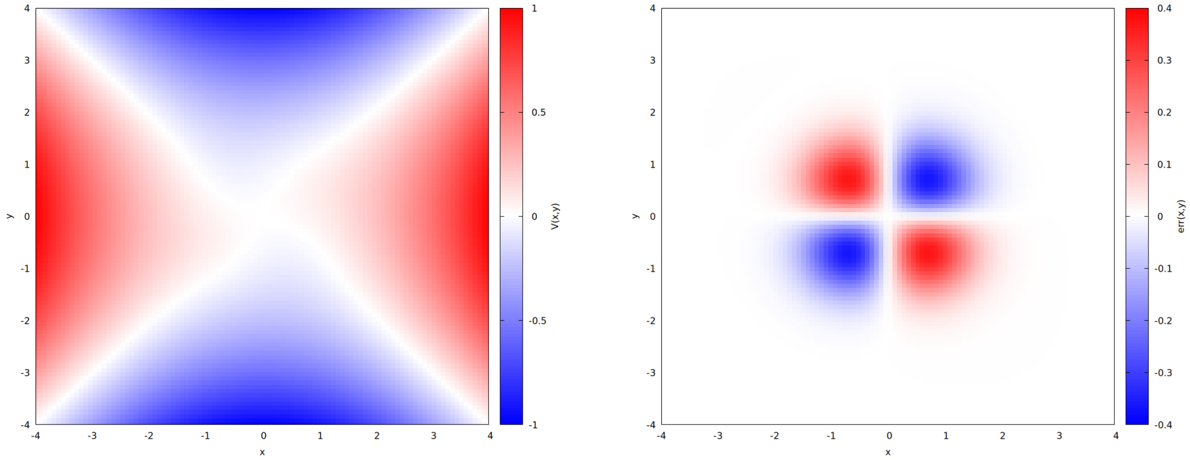

(a) Potential distribution

(b) Error $\nabla^2 V - \frac{\rho}{\epsilon}$

Figure 5: Visualization of potential and its error for inhomogeneous BC